CONF-8910274--2

IRRADIATION EMBRITTLEMENT OF THE SHIPPINGPORT NEUTRON SHIELD TANK*

O. K. Chopra and W. J. Shack

Materials and Components Technology Division
ARGONNE NATIONAL LABORATORY
9700 South Cass Avenue
Argonne, Illinois 60439

CONF-8910274--2

DE90 001942

August 1989

To be presented at the 15th MPA-Seminar on Safety and Reliability of Plant Technology, Stuttgart, FRG, Oct. 5 and 6, 1989, and published in Nuclear Engineering and Design.

*Work supported by the Office of Nuclear Regulatory Research, U. S. Nuclear Regulatory Commission.

IRRADIATION EMBRITTLEMENT OF THE SHIPPINGPORT NEUTRON SHIELD TANK

O. K. Chopra and W. J. Shack

Materials and Components Technology Division, Argonne National Laboratory, 9700 South Cass Avenue, Argonne, IL 60439, U. S. A.

15th MPA-Seminar, October 5 and 6, 1989

The irradiation embrittlement of the Shippingport neutron shield tank material has been characterized. The results indicate embrittlement of the A212 grade B steel from low-temperature, low-flux environment. However, the shifts in Charpy transition temperature are lower than those for the HFIR surveillance samples. The data agree well with results from high flux test reactors. Annealing studies indicate complete recovery of embrittlement after a 2-h anneal at 400°C.

1. Introduction

Surveillance specimens from the High Flux Isotope Reactor (HFIR) at Oak Ridge National Laboratory showed an unexpectedly high degree of embrittlement on the basis of data obtained on similar materials in Materials Testing Reactors (MTRs) [1-3]. One explanation of the difference between the HFIR data and the test reactor data is that, for a given irradiation level, embrittlement is greater at lower flux. Since current guidelines for the assessment of the embrittlement of the pressure vessel support structures of commercial light water reactors do not consider flux, the HFIR results raise the possibilty that they may not be adequately conservative.

To help resolve this issue, a program was initiated to characterize the irradiation embrittlement of the neutron shield tank (NST) from the decommissioned Shippingport reactor. The Shippingport NST operated at 55°C (130°F) and was fabricated from rolled A212 grade B steel, similar to that used for the HFIR vessel. The inner wall of the NST was exposed to a total maximum fluence of ~6×10^{17} n/cm^2 (E>1 MeV) over a life of 9.25 effective full power years. This corresponds to a fast flux of 2.1×10^9 n/cm^2·s, which is comparable to that of the HFIR surveillance specimens.

2. Material Characterization

The effort to obtain samples from the NST was sponsored jointly by the NRC and the DOE Plant Life Extension Program (PLEX) at Sandia National Laboratory. The actual sampling was performed by staff from Pacific Northwest Laboratory. Eight disc samples, ~155 mm in diameter, of the

base metal and three weld samples were obtained from the inner wall of the NST along with the corresponding samples from the very slightly irradiated outer wall. The layout for the sample locations from the inner wall is shown in Fig. 1. The details for sample acquisition are presented elsewhere [4]. The inner wall is constructed from four 25.4-mm thick plates, welded after assembly. Thus, specimen locations 13, 14, and 15 contain vertical welds between the two upper plates and the other locations represent the base metal from the four plates. The total fluence varied among the various locations; the maximum vertical fluence occurred at an elevation of 211.07 m (692.5 ft.), while the maximum azimuthal fluence occurred at the 160 and 340° positions (Fig. 1). The estimated fluence was ~$6x10^{17}$ n/cm^2 (E>1 MeV) for locations 3 and 9, and ~$4x10^{17}$ n/cm^2 for locations 2 and 8 [5,6]. The irradiation levels for the samples from the outer wall are about a factor of 10^6 lower. No effect of irradiation is expected at these low levels and, therefore, the samples from the outer wall were used to determine baseline data for unirradiated material.

The outer wall of the NST was constructed from two plates joined together by vertical welds at azimuthal positions 0 and 180° (north and south welds). A weld sample was obtained from the outer wall at location 1, with a azimuthal position 180° and 210.31 m (690 ft.) elevation.

The available records are not adequate to determine whether all the plates used for the NST were from the same heat of steel. However, metallurgical characterization and chemical analyses of samples taken from each of the plates strongly suggest that both the inner and outer walls of the NST were fabricated from a single heat. Typical chemical analyses for the plate and weld metal are given in Table 1.

Metallographic examination of the NST material indicates that the rolling direction is in the horizontal direction. Micrographs of the grain structure along the rolling and transverse directions are shown in Fig. 2. The surfaces shown in the micrographs are designated by the direction normal to that surface. The transverse section shows some elongated grains and all the inclusions are elongated in the rolling direction. The inclusions in the rolling section are globular or flat.

There are significant variations in hardness across the thickness of the wall. A typical hardness profile (Rockwell B) for the outer wall is shown in Fig. 3a. (The depth is measured from the inner surface of the plate, i. e., the surface towards the reactor core.) The hardness values of the inner and outer regions of the plate are ~10% higher than the plate center. However, no measurable change in grain size was observed across the thickness of the wall; the average through-wall grain size was ~12 μm. Irradiation increases

the hardness of the material, however, the V-shape profile is maintained at most locations, Fig. 3b.

3. Irradiation Embrittlement

The irradiation embrittlement has been characterized by Charpy-impact and tensile tests. Specimens were obtained in the LT and TL orientations* from three regions, i.e., inner, center, and outer 10-mm wide regions, across the thickness of the NST wall. A typical layout for the base metal specimens from the inner and outer walls is shown in Fig. 4. Material from the outer wall, which was protected by ~0.9 m (~3 ft.) of water and hence had a six orders of magnitude lower fluence than the inner wall, was used to obtain baseline data for unirradiated material.

Charpy impact tests were conducted on standard Charpy V-notch specimens machined according to ASTM specification E 23. A Dynatup Model 8000A drop weight impact machine with an instrumented tup and data readout system was used for the tests. Tensile tests were performed on dog bone specimens, with 4 x 5 mm cross section and 20 mm gauge length.

3.1 Base Metal

Charpy transition curves for the LT and TL specimens from different regions of the NST outer wall are shown in Fig. 5. The results indicate that the variation in the transition curves with vertical and azimuthal position is very slight. However, the TL orientation is weaker than the LT orientation. The Charpy transition temperature (CTT) at the 20.7 J (15 ft·lb) level is higher and the upper shelf energy (USE) is lower for the TL specimens. The CTT and USE, respectively, are 16°C (61°F) and 98 J/cm^2 (58 ft·lb) for LT specimens and 19°C (66°F) and 56 J/cm^2 (33 ft·lb) for TL specimens. The differences in impact strength are primarily attributed to differences in the structure of the material. The plane of the crack for TL orientation, i.e., transverse section shown in Fig. 2, contains elongated inclusions which facilitate cleavage by particle cracking.

The results also indicate some effect of position through the thickness of the wall; impact energies for specimens from the inner and outer regions of the wall are comparable while those for the center specimens are slightly higher, Fig. 5b. The CTT and USE for the center specimens are 9°C (48°F)

---

* The first digit designates the direction normal to the plane of the crack and second digit represents the direction of crack propagation. L = longitudinal or rolling direction and T = transverse direction.

and 104 J/cm^2 (61 ft·lb), respectively. This correlates with the differences in the hardness of the material. The hardness of the center region is R_B ~75 (137 DPH) and that of the inner or outer regions is R_B ~83 (159 DPH).

The transition curves for the LT and TL specimens from different positions on the NST inner wall, are shown in Fig. 6. The irradiated inner wall specimens show a higher CTT and lower USE relative to those from the unirradiated outer wall. The transition curves are almost independent of vertical position, which suggests that a factor of 2 to 3 variation in fluence has relatively little effect. For example, the impact energies for specimens from locations 2 and 8 (~4x10^{17} n/cm^2 fluence) are comparable to those for specimens from locations 3 and 9, (~6x10^{17} n/cm^2 fluence). For LT specimens, some differences are observed for specimens from the inner and outer regions of the wall; the shift in CTT is slightly greater for the inner region. The values of CTT are 37°C (99°F) for the outer region and 41°C (106°F) for the inner region; a shift of ~21 and 25°C (~38 and 45°F) for the outer and inner regions, respectively. The USE can not be established from the data in Figs. 6a and 6b. However, the specimens tested at 55°C show 100% shear fracture and, thus, the impact energies for these specimens are representative of USE.

The shift in CTT for the inner wall TL specimens is also 25°C (45°F), similar to that for the LT specimens. However, the actual value of CTT is higher, 44°C (111°F). The effects of material hardness are minimal for the TL specimens. The impact energies for the center specimens are comparable to specimens from the inner and outer region, although the hardness is significantly different, e.g.,R_B ~82 and 88 (156 and 176 DPH) for the center and inner or outer regions, respectively.

Tensile tests on LT specimens from several locations of the NST inner and outer walls were conducted at room temperature and at 55°C. The results indicate a higher yield stress for the inner wall relative to the outer wall, whereas the ultimate stress is approximately the same. The increase in yield stress is ~51 MPa (~7.3 ksi) at room temperature and ~40 MPa (~5.8 ksi) at 55°C. The tensile strength for locations 2 and 8 (~4x10^{17} n/cm^2 fluence) is comparable to that for locations 3 and 9 (~6x10^{17} n/cm^2 fluence.

Hardness influences the tensile properties at both test temperatures, viz., the yield stress for the specimen from the center of the wall is always lower than that for the specimens from inner or outer regions. The difference is ~30 MPa (~4.4 ksi) at room temperature and ~15 MPa (~2.2 ksi) at 55°C. However, the increase in yield stress due to irradiation is the

same for the specimens from the center and from the inner or outer regions of the walls.

The tensile properties of the NST material were also estimated from the Charpy impact data. For dynamic loading, the yield stress is estimated from the expression

$$\sigma_y = AP_yB/Wb^2 , \qquad (1)$$

taken from Ref. 7, where P_y is the yield load obtained from the load-time traces of the instrumented Charpy tests, W is the specimen width, B is the specimen thickness, b is the uncracked ligament, and A is a constant. The constant A was obtained by comparing the tensile and Charpy data for LT specimens tested at room temperature and at 55°C. The best value of the constant was 1.73. The yield loads and the estimated yield stresses for the outer and inner walls are shown in Fig. 7. The measured yield stresses are compared with the estimated values. The results show the expected decrease in yield stress with an increase in test temperature. In the lower shelf temperature regime, cleavage occurs before general yielding and, therefore, the yield loads are very low. For the Charpy impact tests, cleavage fracture occurs when the yield loads are ~13 kN (~1.9 kip). Irradiation increases the yield stress at all test temperatures and, therefore, the CTT shifts to higher temperatures. Irradiation hardening is greater at room temperature than at higher temperatures.

3.2 Weld Metal

Weld samples were obtained at one position on the outer wall and three positions on the inner wall, i.e., locations 14 and 15 with ~$6x10^{17}$ n/cm^2 fluence and location 13 with ~$4x10^{17}$ n/cm^2 fluence. All the welds were transverse to the plate rolling direction. Charpy impact test specimens were machined perpendicular to the weld and from the inner and outer regions across the thickness of the plate. The impact strength of the outer wall weld is significantly higher than that of the base metal, Fig. 8a. The 41 J (30 ft·lb) CTT and USE for the weld are -2°C (28°F) and 182 J/cm^2 (107 ft·lb), respectively. Location through the thickness of the weld has little or no effect on the transition curve.

The inner wall specimens show significant effect of position around the wall as well as through the thickness of the wall. The impact energies for weld specimens from the outer region of positions 13, 14, and 15 are comparable but slightly higher than those for the outer wall weld specimens, Fig. 8b. The transition curves for the inner region of the inner wall welds are shown in Figs. 8c and 8d. The 40 J CTT is 8°C (46°F) for location 13

and 15 welds and 23°C (73°F) for location 14 weld, i.e., a shift of 10 and 25°C, respectively, for the two data sets. The results for the outer weld may not be representative of the unirradiated inner wall welds. The chemical compositions of weld metal from different locations indicate only minor variations in silicon and copper contents, Table 1. Additional tests and metallographic characterization of the welds are being performed to better establish the transition curves. Annealing studies are also planned to obtain the baseline data and determine the embrittlement behavior of the welds.

4. Recovery Annealing

Annealing studies were conducted on material from the NST inner and outer walls to study the recovery behavior of the embrittled material. Specimens were annealed at 400°C (752°F) for up to 154 h and the annealing behavior characterized by hardness measurements. The results indicate that the hardness of irradiated material from the inner shell decreases after annealing, while the outer shell material shows an increase in hardness. Annealing for 1 h at 400°C is sufficient for recovery; there is a very slight increase in hardness of both the inner and outer shell materials after annealing for longer times. The changes in hardness for material from inner and outer shells are shown in Fig. 9. The hardness changes reflect the differences in the fluence and flux levels for the different locations, i.e., the decrease for locations 3 and 9 is greater than for location 8.

Charpy impact data for TL specimens from the NST inner and outer walls, annealed for 2 h at 400°C, are shown in Fig. 10. The results indicate a complete recovery of irradiation embrittlement, i.e., the transition curve for the annealed specimens from the inner wall is identical to that for the outer wall. Annealing has little or no effect on the transition curve for the outer wall, Fig. 10b.

5. Discussion

Charpy-impact and tensile data for the Shippingport NST indicate that the shift in CTT is not as severe as would be expected on the basis of the changes seen in HFIR surveillance samples. Charpy transition curves for the NST outer and inner walls are compared with the results for unirradiated and irradiated HFIR surveillance samples in Fig. 11. Although the shift is smaller the actual CTT for the NST material is significantly higher than that for the HFIR material. The impact energy for the NST inner wall is very low,~40 J/cm^2 (24 ft·lb), at the service temperature of 55°C (130°F).

Except for minor differences in copper and nickel contents, the chemical compositions of the two materials are comparable. The

concentrations of copper and nickel are 0.15 and 0.20 wt.%, respectively, for HFIR material and 0.05 and 0.04 wt.% for NST. Although the HFIR material is tougher than the NST material, the tensile strength of the HFIR material is greater than the NST material. The yield strength and hardness, respectively, are 355±11 MPa (48.6±1.6 ksi) and 170 DPH [2] for the HFIR material and 305±19 MPa (44.2±2.8 ksi) and 159 for NST. The difference in the transition curves for the two unirradiated materials is most likely due to microstructural factors, such as the amount and distribution of inclusions.

When the shifts in CTT for the NST material are compared with the results for the HFIR material irradiated in the ORR and other A212B steels irradiated in high flux test reactors, Fig. 12, the results for Shippingport NST are consistent with the test reactor data. The results for the NST material also agree very well with correlations for the shift in CTT, increase in tensile yield stress, and the increse in hardness, developed for pressure vessel steels [8-10]. The shift in transition temperature, ΔT, with an increase in tensile yield stress, $\Delta\sigma_y$, is expressed as

$$\Delta T = C\Delta\sigma_y , \qquad (2)$$

where C~0.5 °C/MPa for the plate material and 0.65 °C/MPa for welds. The change in yield stress with hardness, ΔDPH, is given by the relation

$$\Delta\sigma_y = 3.5\Delta DPH . \qquad (3)$$

The shift in CTT for both LT and TL specimens is 25°C (45°F) and the increase in yield stress is 51 MPa (7.3 ksi). The increase in hardness due to irradiation is difficult to obtain because of the variation in hardness across the thickness of the wall. However, annealing studies indicate that the irradiation-induced hardness change, represented by the decrease in hardness after annealing at 400°C for 2 h, is ~4.3 R_B (14 DPH) for locations 3 and 9. This is consistent with Eq. (3). The change in hardness is slightly lower, i.e., ~3.5 R_B, for location 8.

The results from the present study suggest that the unexpectedly high embrittlement for the HFIR surveillance samples may not be due to flux effects but is caused by other factors. The minor differences in copper and nickel contents between the two materials are not expected to have any effect at the low irradiation temperatures for Shippingport NST and HFIR. However, the effects of the differences in the neutron spectrums at Shippingport and HFIR [6] require futher investigation. High flux irradiation experiments are planned on Shippingport NST and HFIR vessel materials, to evaluate the possible effects of metallurgical differences between the two materials.

6. Conclusions

Characterization of material from the Shippingport neutron shield tank indicates that the embrittlement of the A212 grade B steel in the low-temperature, low-flux environment is consistent with that expected from the current NRC regulatory guidelines. However, the shifts in Charpy transition temperature are lower than those for the HFIR surveillance samples. The reasons for this difference are not well understood at present.

The data on the weld samples from the NST indicate that the weld metal is tougher than the plate material. The results, however, show significant scatter and irradiation embrittlement could not be characterized. Annealing studies are planned to investigate the recovery behavior of the weld metal and to obtain additional information on the shift in Charpy transition temperature.

Acknowledgements

This work was supported by the Office of Nuclear Regulatory Research, U. S. Nuclear Regulatory Commission. The authors are grateful to W. F. Burke and G. M. Dragel for their experimental contributions and to A. Sather for conducting the mechanical tests.

References

1. R. K. Nanstad, K. Farrel, D. N. Braski, and W. R. Corwin, Accelerated Neutron Embrittlement of Ferritic Steels at Low Fluence: Flux and Spectrum Effects, J. Nucl. Mater. 158 (1988) 1.

2. R. D. Cheverton, J. G. Merkle, and R. K. Nanstad, Evaluation of HFIR Pressure Vessel Integrity Considering Radiation Embrittlement, Oak Ridge National Laboratory Report, ORNL/TM-10444 (April 1988).

3. J. R. Hawthorne, Studies of Radiation Effects and Recovery of Notch Ductility of Pressure Vessel Steels, British Nuclear Energy Conference, Iron and Steel Institute, London, England (1960).

4. S. T. Rosinski, O. K. Chopra, and W. J. Shack, Shippingport Neutron Shield Tank Sampling and Analysis Program, Proc. 1989 Pressure Vessel and Piping Conf., Honolulu, July 23-27, 1989, to be published.

5. R. M. Allen, Technical Support Document LWBR Reactor Vessel Assembly, Bettis Atomic Power Laboratory Report, WAPD-LP(RC)SE-140 (November 1977).

6. L. James, Bettis Atomic Power Laboratory, Private Communication (April 1989).

7. W. L. Server, Impact Three-Point Bend Testing for Notched and Precracked Specimens, J. Testing and Evaluation, Vol. 3, No. 1 (1978) 29.

8. G. R. Odette, R. A. Wullaert, and P. Lombrozo, Some Observations to the Relation Between Strengthening and Embrittlement of Irradiated Pressure Vessel Steels, J. Nucl. Mater.

9. G. R. Odette and G. E. Lucas, Irradiation Embrittlement of Reactor Pressure Vessel Steels: Mechanisms, Models and Data Correlation, ASTM-STP-909, American Society for Testing and Materials (1986) 206.

10. G. E. Lucas and G. R. Odette, Recent Advances in Understanding Radiation Hardening and Embrittlement Mechanisms in Pressure Vessel Steels, Proc. Second Intl. Symp. on Environmental Degradation of Materials in Nuclear Power Systems - Water Reactors, American Nuclear Society, TMS-AIME-NACE, Monterey, CA. (September 1985) 345.

Table 1. Typical Chemical Compositions (wt.%) of the A212 Grade B Plate and Weld Metal from the Shippingport Neutron Shield Tank

Element	Plate	Weld
C	0.23	
Mn	0.76	0.93
P	0.02	-
S	0.03	-
Si	0.27	0.73[1]
Cu	0.05	0.06[2]
Ni	0.04	0.02
Cr	0.04	0.03
O	0.01	
N	0.004	
Ti	<0.005	0.025
V	<0.005	0.019
Zr	<0.005	<0.005
Mo, Ca, Al	<0.01	<0.01
B, Se, Sn	<0.01	<0.01

[1] 0.86 for inner wall weld from location 14.

[2] 0.07 for outer wall weld and 0.04 for inner wall weld from location 15.

Figure 1. Cylindrical Development of the Shippingport Neutron Shield Tank Inner Wall

Figure 2. Micrographs of the NST Material Along the (a) Transverse and (b) Rolling Sections.

Figure 3. Hardness Profile across the Thickness of the (a) NST Outer Wall and (b) Locations 9 of the NST Inner Wall.

Figure 4. Cutting Diagram for Base Metal Samples from the NST inner and outer walls.

Figure 5. Charpy Impact Test Data for the NST Outer Wall. LT specimens from (a) inner and outer regions and (b) center region. TL specimens from (c) inner and outer regions.

Figure 6. Charpy Impact Test Data for the NST Inner Wall. LT specimens from (a) inner and (b) outer region. TL Specimens from (c) inner and outer regions and (d) center region.

Figure 7. Yield Stress Estimated from the Charpy Impact Data for the NST (a) Outer and (b) Inner Walls.

Figure 8. Charpy Impact Test Data for Weld Metal Specimens from (a) NST Outer Wall, (b) Inner Wall Outer Region, and (c) and (d) Inner Wall Inner Region.

Figure 9. Change in Hardness of the Neutron Shield Material from Inner and Outer Walls after Annealing at 400°C.

Figure 10. Charpy Impact Test Data for Annealed TL Specimens from (a) Inner Wall and (b) Outer Wall.

Figure 11. Comparison of Charpy Impact Data for (a) Unirradiated and (b) Irradiated Shippingport NST and HFIR Surveillance Samples.

Figure 12. Comparison of Transition Temperature Shifts for Shippingport NST with HFIR Surveillance Results and A212B data from High Flux Test Reactors.

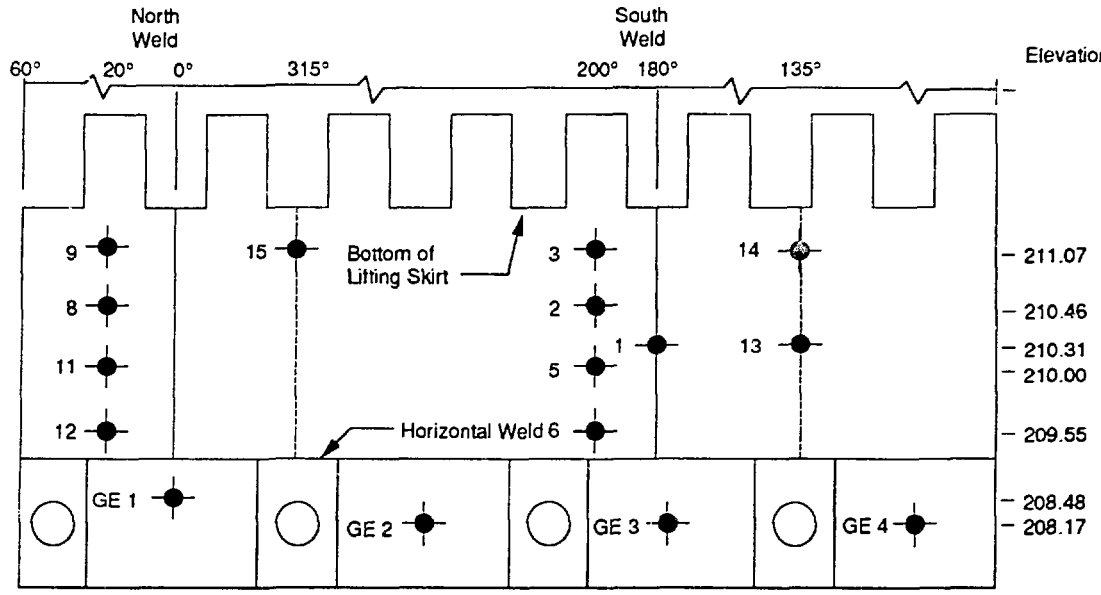

Figure 1. Cylindrical Development of the Shippingport Neutron Shield Tank Inner Wall

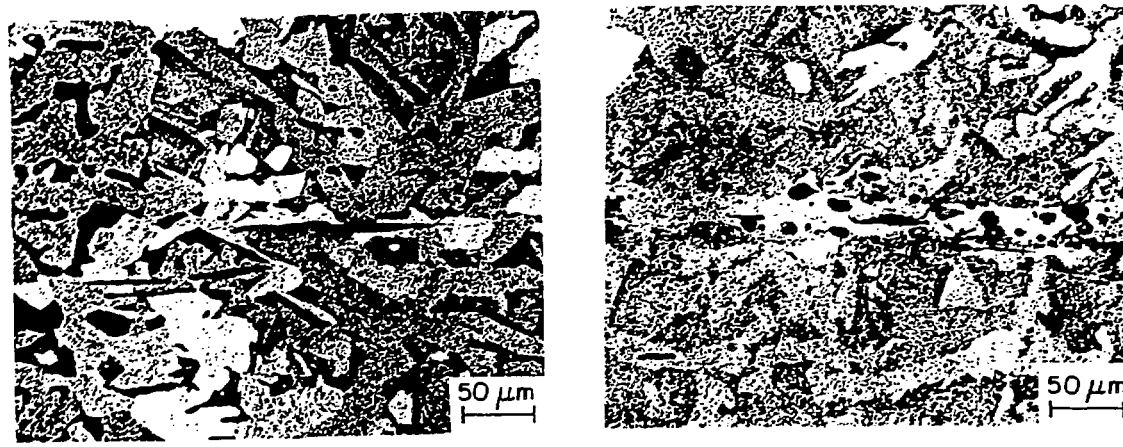

Figure 2. Micrographs of the NST Material Along the (a) Transverse and (b) Rolling Sections.

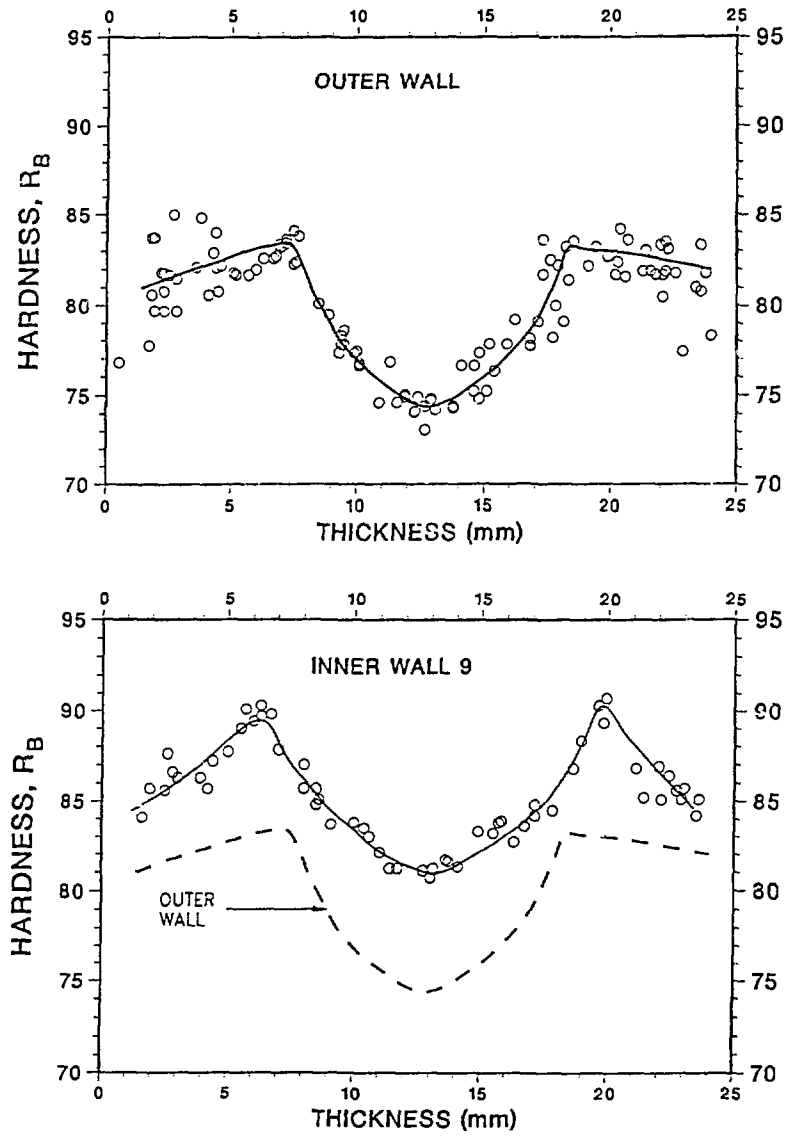

Figure 3. Hardness Profile across the Thickness of the (a) NST Outer Wall and (b) Locations 9 of the NST Inner Wall.

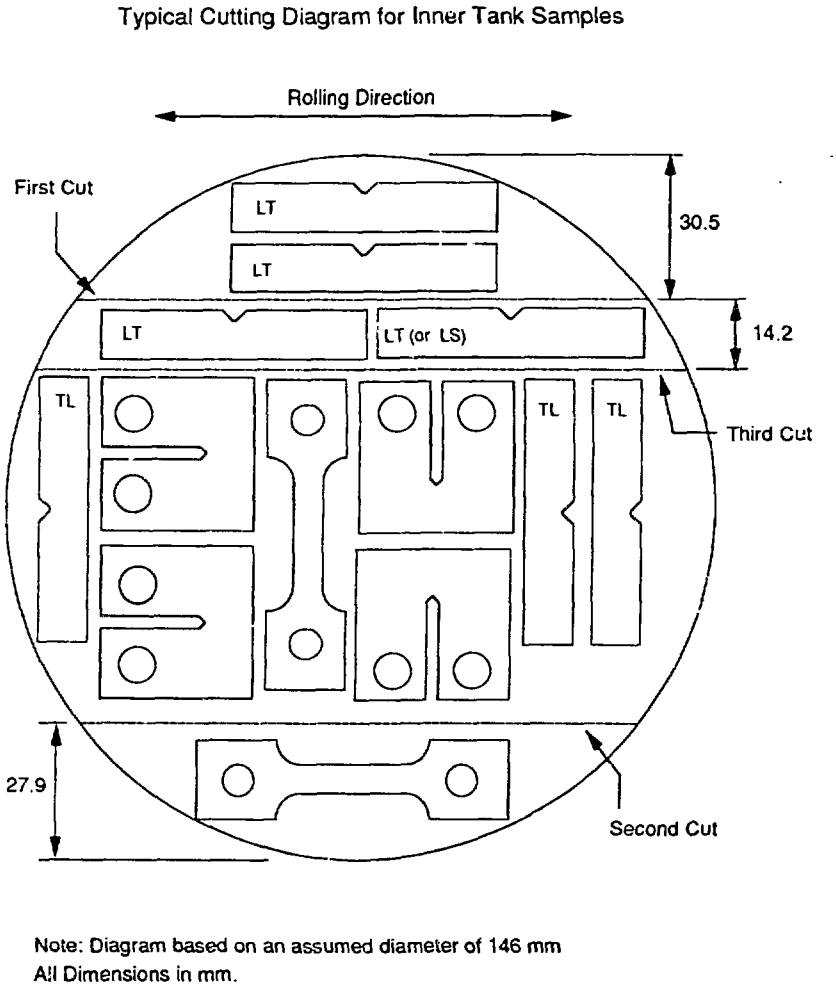

Figure 4. Cutting Diagram for Base Metal Samples from the NST inner and outer walls.

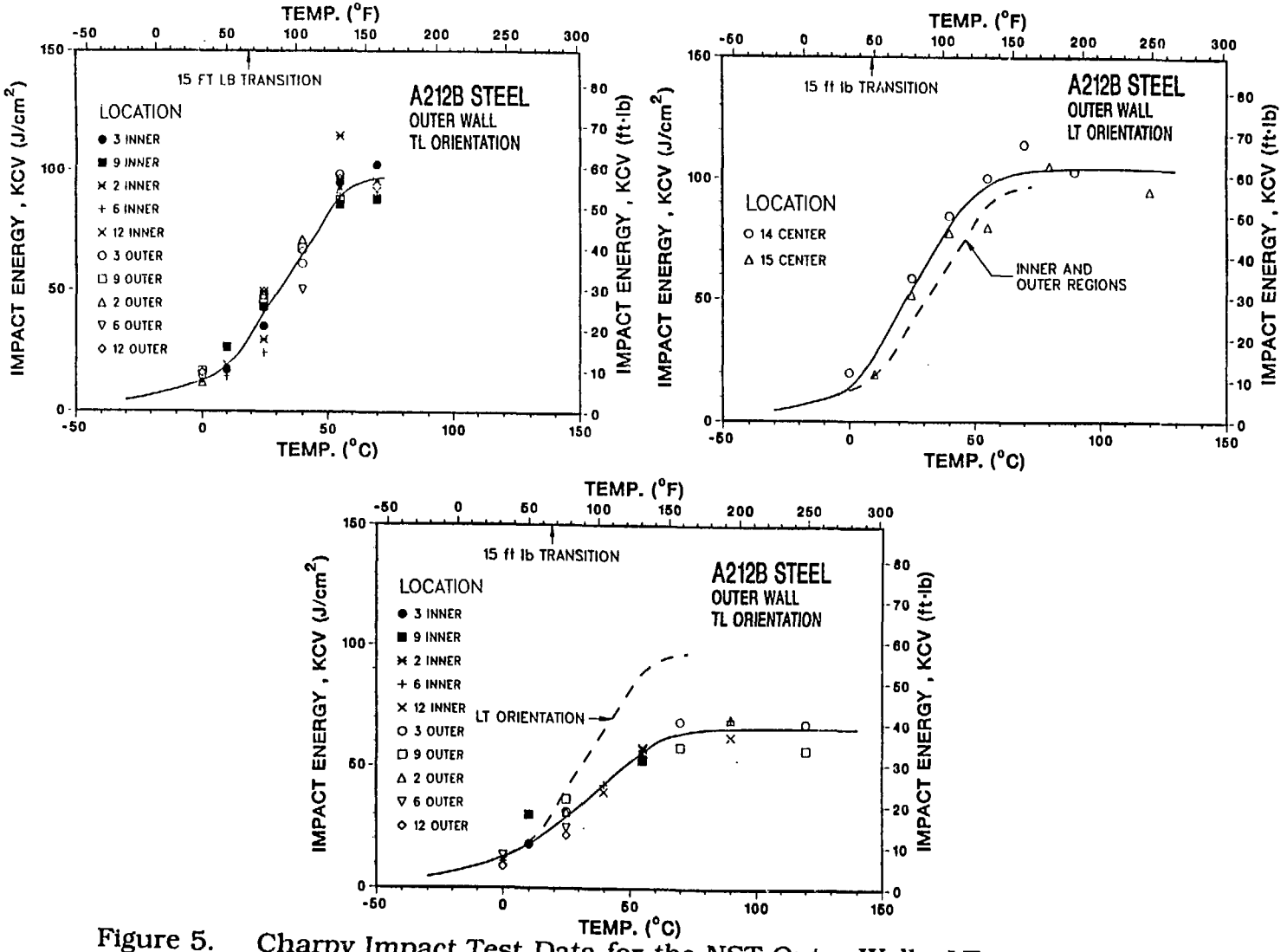

Figure 5. Charpy Impact Test Data for the NST Outer Wall. LT specimens from (a) inner and outer regions and (b) center region. TL specimens from (c) inner and outer regions.

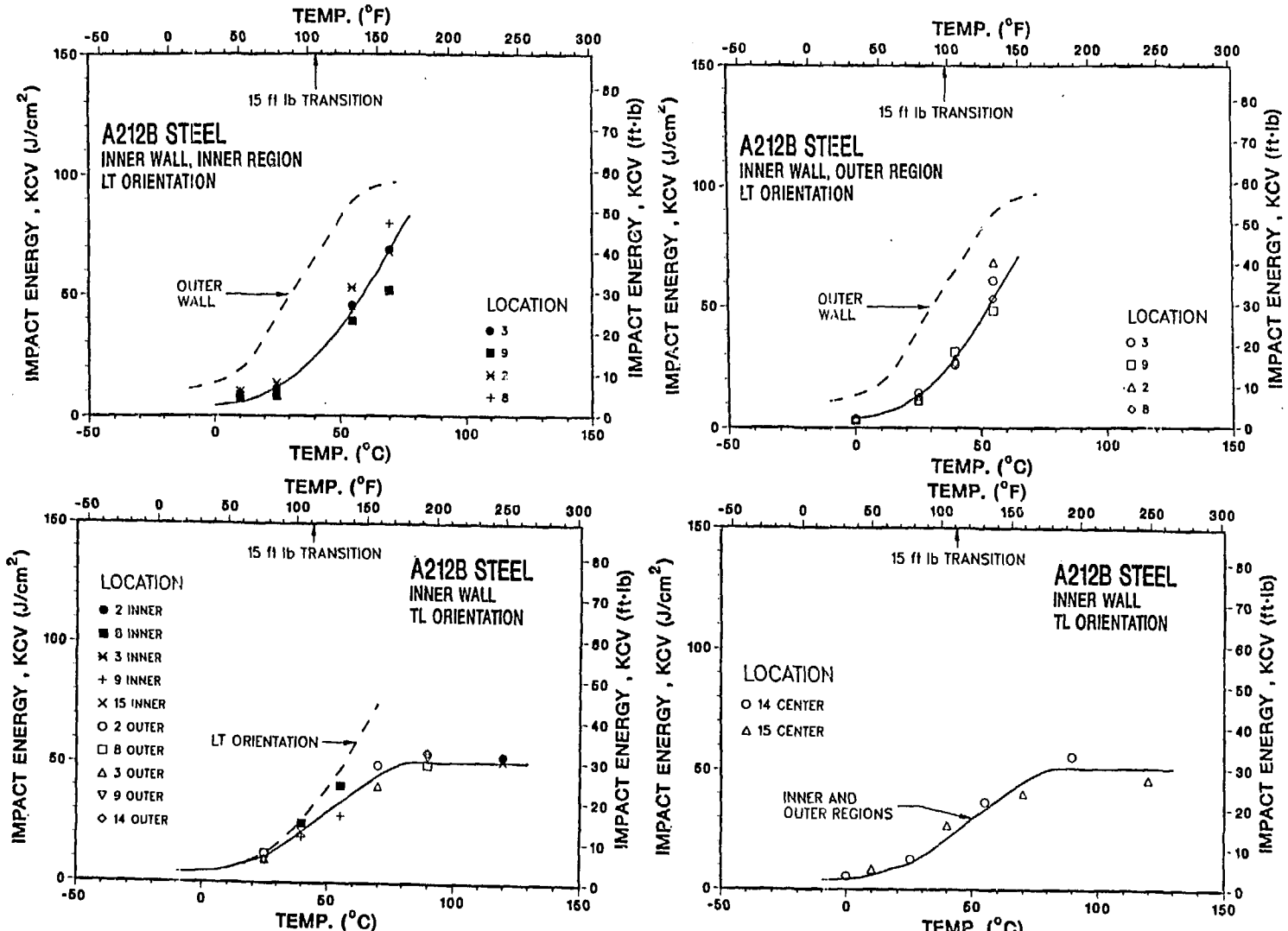

Figure 6. Charpy Impact Test Data for the NST Inner Wall. LT specimens from (a) inner and (b) outer region. TL Specimens from (c) inner and outer regions and (d) center region.

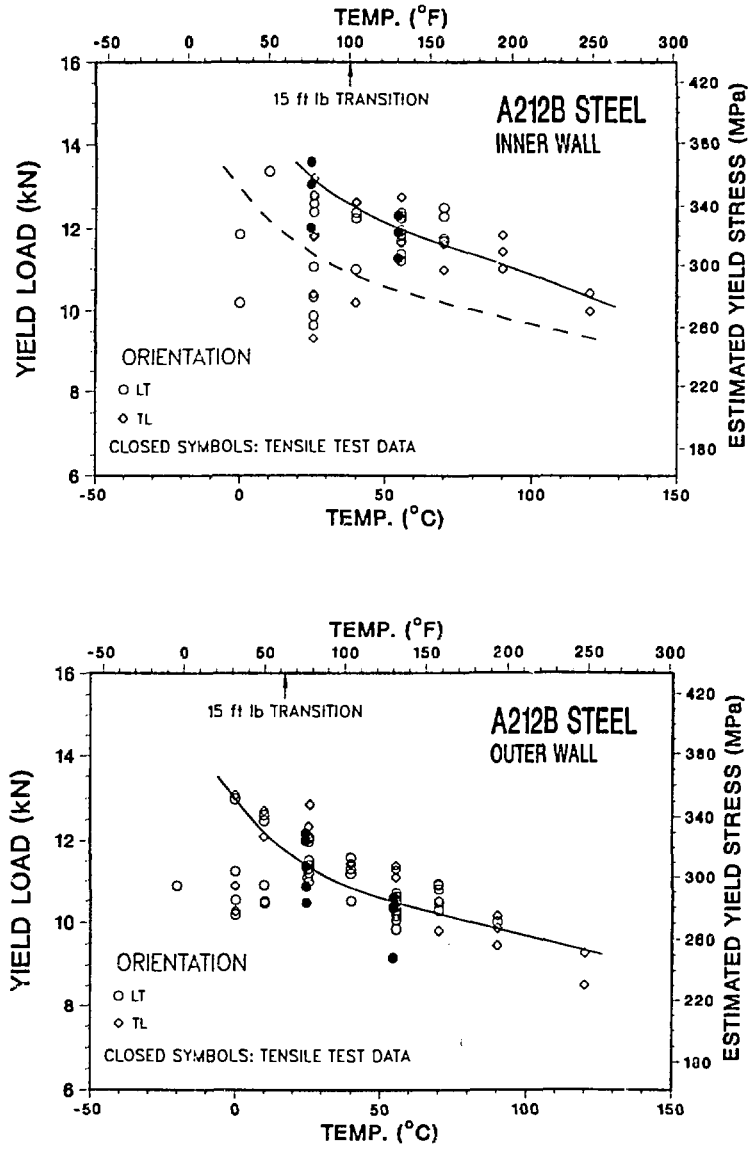

Figure 7. Yield Stress Estimated from the Charpy Impact Data for the NST (a) Outer and (b) Inner Walls.

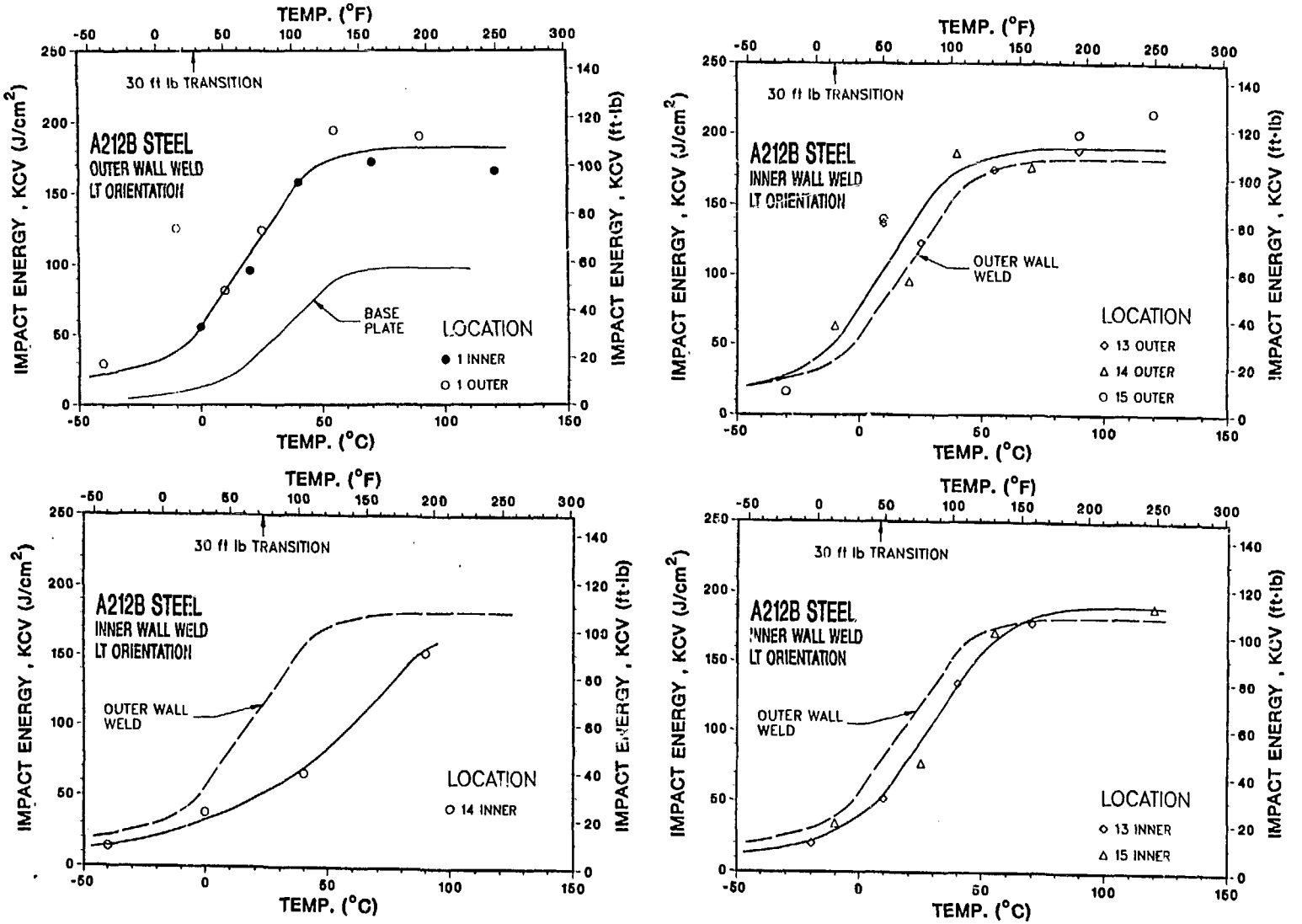

Figure 8. Charpy Impact Test Data for Weld Metal Specimens from (a) NST Outer Wall, (b) Inner Wall Outer Region, and (c) and (d) Inner Wall Inner Region.

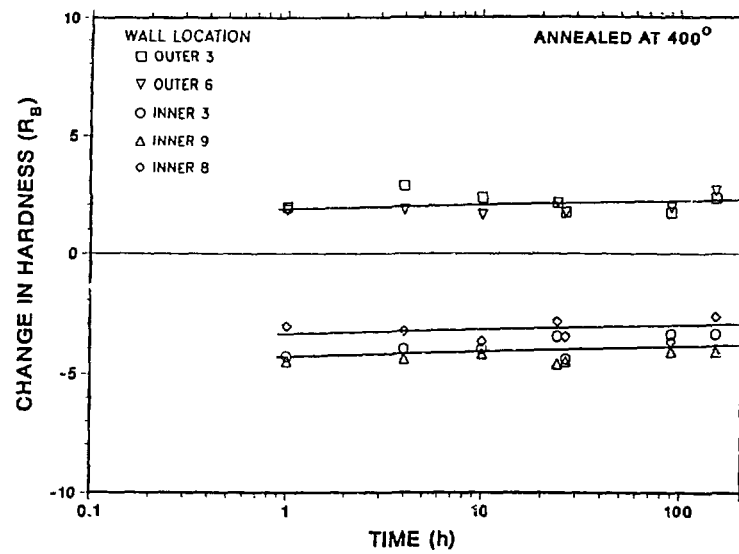

Figure 9. Change in Hardness of the Neutron Shield Material from Inner and Outer Walls after Annealing at 400°C.

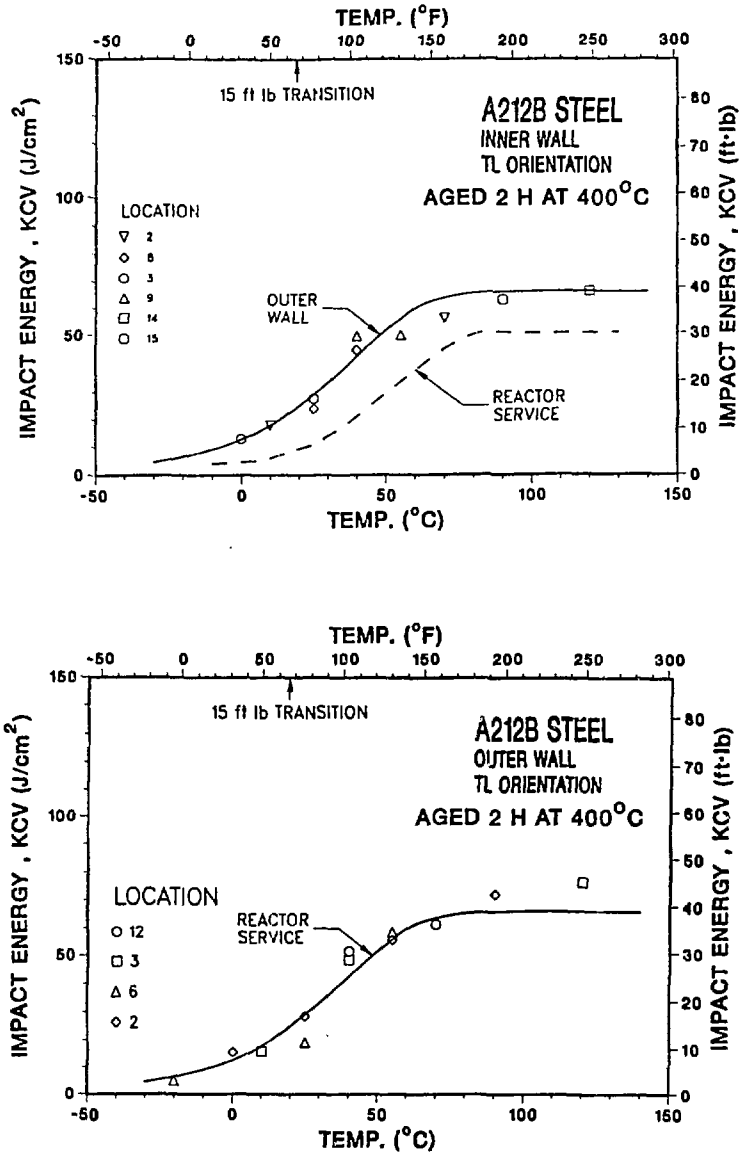

Figure 10. Charpy Impact Test Data for Annealed TL Specimens from (a) Inner Wall and (b) Outer Wall.

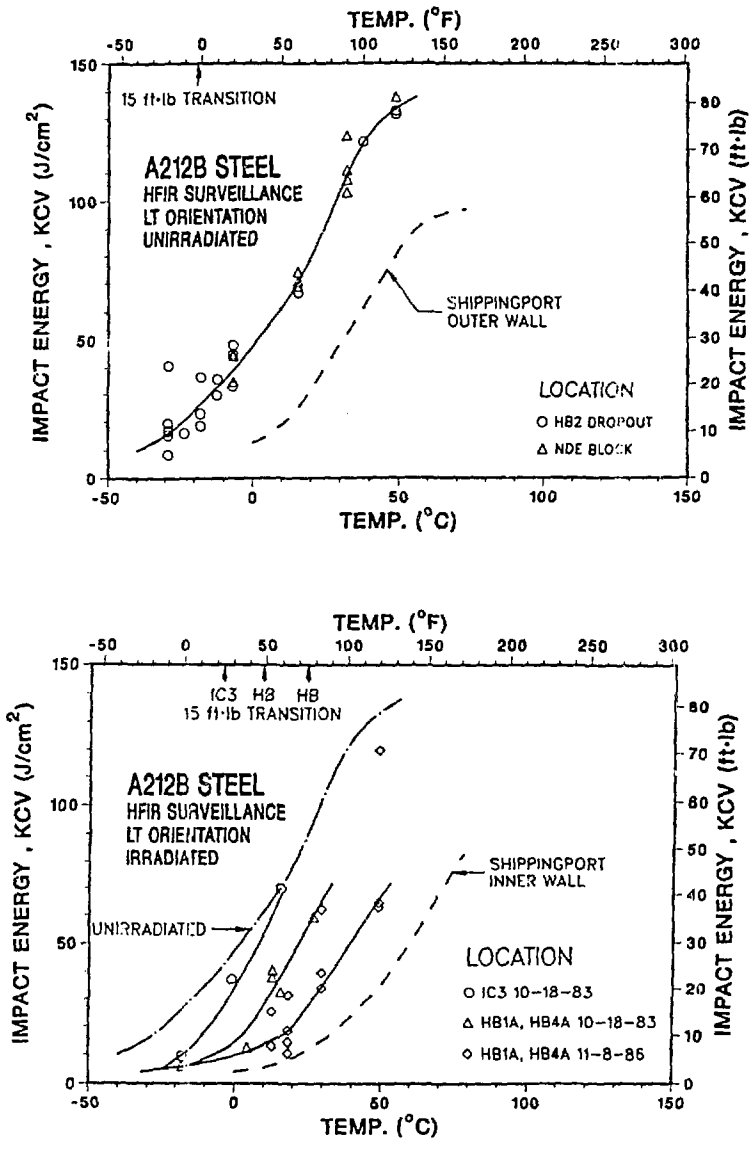

Figure 11. Comparison of Charpy Impact Data for (a) Unirradiated and (b) Irradiated Shippingport NST and HFIR Surveillance Samples.

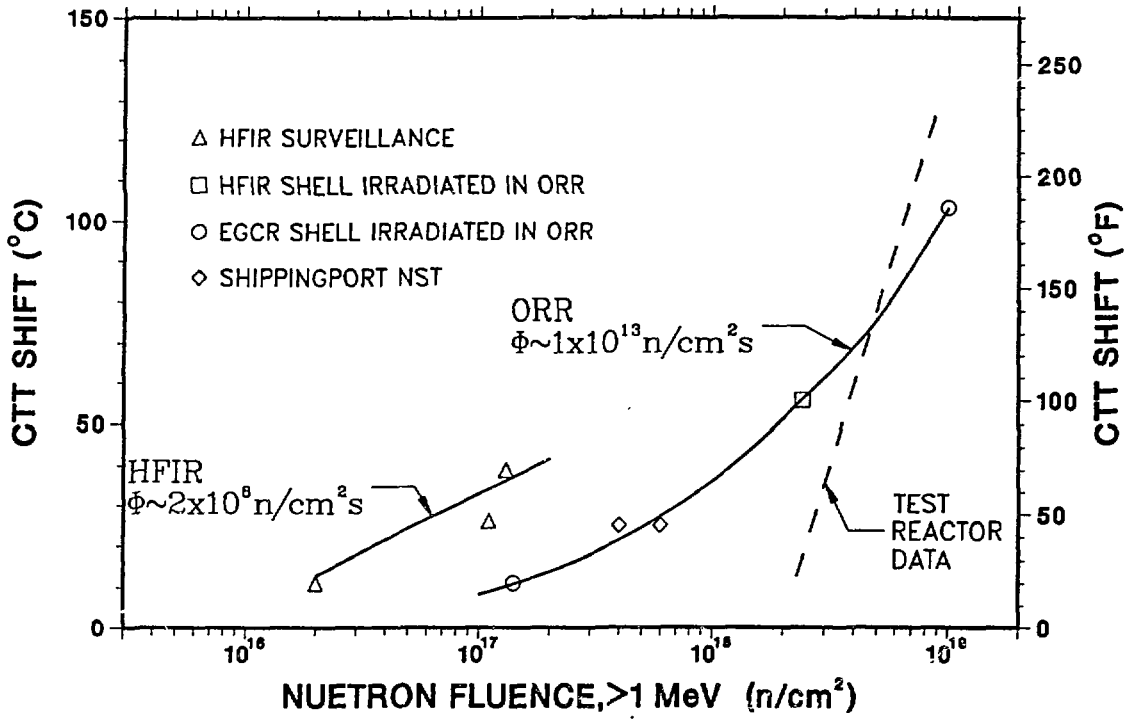

Figure 12. Comparison of Transition Temperature Shifts for Shippingport NST with HFIR Surveillance Results and A212B data from High Flux Test Reactors.